Rev. Roum. Sci. Techn.– Électrotechn. et Énerg.
Vol. **69**, *4*, pp. 407–412, Bucarest, 2024

DANDELION OPTIMIZATION-BASED MODIFIED ULTRA SPARSE MATRIX CONVERTER FOR UNBALANCED AND HARMONIC GRID

WENCHESLAUS VINIL DANI [1, *], MICHAEL CHRISTUDHAS JOBIN CHRIST [2]

Keywords: Ultra-sparse matrix converter; Dandelion optimization; Current space vector modulation method; Z-source network; Doubly fed induction generator.

Variations in wind speed led to a non-constant power output from the wind energy conversion system (WECS). With wind energy penetration into utility grids increasing, there are challenges in the power quality of the electricity supply. Several existing techniques have been introduced; however, they are challenged by harmonics in wind power output from WECS and traditional matrix converters, which are inefficient due to their high switch count, low voltage transfer ratio, and sensitivity to changing conditions. In this research, a modified ultra-sparse matrix converter (MUSMC) has been proposed to improve the quality of wind power and feed the power to the grid. A modified ultra-sparse matrix converter configuration is designed for power transfer from the WECS to the grid. A dandelion closed-loop-based optimization (DLO) method is presented for injecting harmonically less electricity from wind power systems into the grid. The suggested DLO-based MUSMC system is designed to provide a voltage gain ranging from 0.8 to unity. The proposed system's performance is simulated in MATLAB/Simulink R2021a and tested while considering grid harmonics, an unbalanced grid, and changes in modulation schemes. According to the simulation findings, the suggested modular control approach with the MUSMC performs well under all three test situations, and the FFT analysis demonstrates the control strategy's superiority. This proposed methodology decreases the system's losses, size, and cost.

1. INTRODUCTION

With increased demand for electricity and concern about the impact of fossil fuels on the environment, the necessity of generating power from renewable energy like hydroelectric, tidal, solar, geothermal, and wind has earned more emphasis in recent years [1]. In the WECS, the wind's kinetic energy is turned into electricity utilizing generators [2]. Therefore, wind power is an effective alternative to fossil fuels. Two kinds of generators are used in WECS [3–5]. Usually, an AC-DC-AC converter [6] or the AC-AC [7] converter delivers energy from the generator unit to the grid. The traditional matrix converter [8] uses more switching devices, and the control scheme becomes more complex as the switch count increases.

Moreover, the traditional matrix converter has a poor voltage transfer ratio, reduced reactive power transfer capability, and is sensitive to changes in unpredictable circumstances. To address these limitations, the researchers developed the very sparse matrix converter [10], ultra-sparse matrix converter [9], and sparse matrix converter [11]. Because of the increased switch count, typical matrix converters are more expensive than UMSC.

Another issue related to implementing a conventional matrix converter (CMC) in WECS is the voltage transformation ratio [12]. At first, the venturi modulation method [13] was introduced for operating the conventional matrix converter. This method gives a voltage transformation ratio of less than 0.5. Later, the scalar method [14] was introduced for the traditional matrix converter to improve the voltage transformation ratio, and a voltage transformation ratio of 0.86 was achieved. The overmodulation method [15] gives a high gain value approximately equal to 1. To increase the voltage transformation ratio, two low-frequency transformers are connected in a cascaded manner [16] to the matrix converter circuit. The authors in [17] presented a buck-boost type of matrix converter with a step-change in frequency.

Some control methods like the fractional order PID controller [18], sliding mode control [19] (SMC), cascaded control [20] (CC), fuzzy controller (FC) [21], and voltage mode control are used in the WECS to inject the harmonic less power into the grid. The cascaded controller falls short in only one case: using a conventional PI controller [22]. The authors of [23] describe a moth flame optimizer for optimizing controller parameters. This sturdy controller limits accuracy and convergence while operating the system under dynamic situations. A genetic method with BP (backpropagation) neural network PID control [24] is used for renewable energy applications. The suggested hybrid controller performs exceptionally well under various operating situations [32–35]. A Grasshopper optimization algorithm-based FOPID controller [25] is developed for the hybrid WECS. The system is evaluated for unexpected load variations and volatility in input sources. A comparison analysis of other optimization strategies is performed. In WECS, the rotor speed of the DFIG is controlled using a genetic algorithm-based PID controller [26]. The results show that the GA-PID controller effectively manages the DFIG's speed [27].

In [28], field-oriented manipulators (FOCs) for wind turbines with double-fed induction generators (DFIGs) are demonstrated in real time. As a result of the proposed manipulation, the overall efficiency and total harmonic distortion on the stator-injected energy to the grid are excellent, and the THD on the stator-injected energy is reduced—double-fed induction generators power wind turbines' field-oriented control system (FOC) [29]. An FOC-Hysteresis contemporary controller (HCC) with the stator and resistive load improves manipulative regulation in a rotor side converter (RSC). Results show that the recommended control is excellent in steady and transient modes. WECS includes a permanent magnet synchronous generator (PMSG) designed to benefit from Direct matrix converters (DMC) [30]. The results are satisfactory with using the DMC framework, with more control over the WECS.

From the literature, the following problems related to the WECS have been found: (i) The main disadvantage of using a conventional matrix converter is that it requires more switches, and (ii) the use of conventional modulation methods in WECS affects the control complexity, filter design, switching frequency, sampling frequency, and dynamic response of the system. To solve this issue, this paper presents the implementation of a modular ultra-sparse matrix converter for integrating the DFIG with the grid using a modular control method. In this research, a modified ultra-sparse matrix

[1] St.Peter's College of Engineering and Technology,Avadi, Chennai.India, E mail: vinildani@spcet.ac.in
[2] Rajalakshmi Engineering College Thandalam, Mevalurkuppam, Tamil Nadu, India. E-mail: jobinchrist.mc@rajalakshmi.edu.in

DOI: 10.59277/RRST-EE.2024.69.4.7

converter (MUSMC) has been proposed to improve the quality of wind power to the grid. From the issues presented above, the contributions of the research are as follows:

- We have designed a modified ultra sparse matrix converter (USMC) with high-power transmission capacity and fewer losses. Integrate the Z-source network with the modified USMC to achieve a high voltage transformation ratio.
- The current space vector modulation (CSVM) is implemented for the USMC, and a closed-loop Dandelion optimization (DLO) based SVM control technique is implemented for the grid side converter.
- Compare the efficiency of the WECS with conventional and the proposed MC under various wind speeds and modulation methods.

The paper is constructed as follows: section 2 discusses the modeling of the USMC; section 3 offers the loss analysis of the proposed approach to the conventional framework; section 4 describes a DLO-based closed-loop control strategy for injecting harmonic-less electricity into the grid; and section 5 displays the proposed system's simulation findings. Finally, section 6 summarizes the recommended work.

2. MODELING OF MODULAR ULTRA-SPARSE MATRIX CONVERTER (MUSMC)

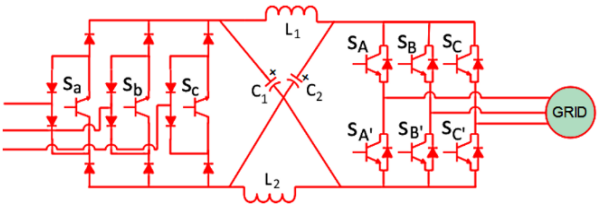

Fig. 1 – Modular ultra-sparse matrix converter.

The DFIG's AC power is converted to DC using three switches and twelve diodes. The upper and lower diode elements are switched depending on the 'OR' gate operation.

The following equation calculates the duty cycle ratio [31, 32] of the two nearby effective vectors required to construct the reference input current vector I_{ref}.

$$\begin{cases} \delta_{\mathrm{m}} = \dfrac{\sin\left[\frac{\pi}{3} - z - \frac{\pi}{6} + \frac{\pi}{3}(\nabla_s - 1)\right]}{\cos\left[z - \frac{\pi}{3}(\nabla_s - 1)\right]} \\ \delta_{\mathrm{n}} = \dfrac{\sin\left[z + \frac{\pi}{6} - \frac{\pi}{3}(\nabla_s - 1)\right]}{\cos\left[z - \frac{\pi}{3}(\nabla_s - 1)\right]} \end{cases} \quad (1)$$

where ∇_s stands for sector number, 'z' denotes the angular location of the reference vector. When the reference cutting-edge drops inside the first sector, the significance of the DC hyperlink voltage is given by:

$$U_{\mathrm{dc}} = \delta_{\mathrm{m}} U_{\mathrm{ab}} + \delta_{\mathrm{n}} U_{\mathrm{ac}} = \frac{3U_{\mathrm{in}}}{2\cos z}, \quad (2)$$

where U_{in} is the magnitude of the input phase voltage, U_{ab}, and U_{ac} are the input line voltages.

3. LOSS ANALYSIS OF PROPOSED DLO-BASED MUSMC

The proposed system is made up of a rectifier and an inverter unit. The switching losses are zero since the current SVM approach triggers the rectifier unit's switches. Figure 1 presents the DLO-based control system. Therefore, the conduction losses of IGBT and diodes are

$$P_{\mathrm{cond\_rec}} = 2P_{\mathrm{cond\_UGBT\_rec}} + 4P_{\mathrm{cond\_diode\_rec}}, \quad (3)$$

$$\begin{cases} P_{\mathrm{cond\_UGBT\_rec}} = \frac{1}{2\pi}\int_0^{2\pi} \mathrm{d}E_{\mathrm{IGBT}} \\ P_{\mathrm{cond\_diode\_rec}} = \frac{1}{2\pi}\int_0^{2\pi} \mathrm{d}E_{\mathrm{diode}} \end{cases}, \quad (4)$$

$$\begin{cases} E_{\mathrm{IGBT}} = V_{\mathrm{cc(sat)}} I_{\mathrm{dc}} T_{\mathrm{s}} = \left(V_{\mathrm{ce(0)}} I_{\mathrm{dc}} + r_{\mathrm{cc}} {I_{\mathrm{dc}}}^2\right) T_{\mathrm{s}} \\ E_{\mathrm{diode}} = V_{\mathrm{D(sat)}} I_{\mathrm{dc}} T_{\mathrm{s}} = \left(V_{\mathrm{D(0)}} I_{\mathrm{dc}} + r_{\mathrm{D}} {I_{\mathrm{dc}}}^2\right) T_{\mathrm{s}} \end{cases}, \quad (5)$$

$$I_{\mathrm{dc}} = P_{\mathrm{o}}/U_{\mathrm{dc}} = \sqrt{3} U_{\mathrm{om}} I_{\mathrm{om}} \cos(\varphi_{\mathrm{o}})/U_{\mathrm{dc}}. \quad (6)$$

where, E_{IGBT} represents the energy dissipated by the IGBT during conduction, E_{diode} represents the energy dissipated by the diode during conduction. I_{dc} denotes the DC flowing through the circuit, T_{s} is switching period, r_{cc} is the IGBT's on-state resistance, the diode resistance. P_{o} stands for output power, $U_{\mathrm{om}} and\ I_{\mathrm{om}}$ stands for output voltage and current magnitude. Total conduction losses of USMC rectifier stage (Pcond_rec)

$$\frac{4\sqrt{3} I_{\mathrm{om}} m_{\mathrm{c}} cos(\varphi_{\mathrm{o}})}{\pi}\left(V_{\mathrm{ce(0)}} + 2V_{\mathrm{D(0)}}\right) + \\ + \frac{(4\pi + 6\sqrt{3}) \cdot I_{\mathrm{om}}^2 m_{\mathrm{c}}^2 \cos^2(\varphi_{\mathrm{o}})}{3\pi}\left(r_{\mathrm{ce}} + 2r_{\mathrm{D}}\right). \quad (7)$$

The switching loss and conduction loss of the inverter stage are presented in the equations

$$P_{\mathrm{sw_{inv}}} = \frac{6}{\pi} f_{\mathrm{c}} \left(E_{\mathrm{on\ IGBT}} + E_{\mathrm{off\_IGBT}} + E_{\mathrm{off\_D}}\right) \frac{U_{\mathrm{dc}}}{v_{\mathrm{ref}}} * \frac{I_{\mathrm{om}}}{I_{\mathrm{ref}}}, \quad (8)$$

$$\begin{cases} P_{\mathrm{ound\_KGBT\_inv}} = V_{\mathrm{cec(0)}} I_{\mathrm{om}} \left(\frac{1}{2\pi} + \frac{m_{\mathrm{v}} \cos(\varphi_{\mathrm{o}})}{8}\right) \\ \quad + r_{\mathrm{ce}} I_{\mathrm{cm}}^2 \left(\frac{1}{8} + \frac{m_{\mathrm{v}} \cos(\varphi_{\mathrm{o}})}{3\pi} + 2\pi F_{\mathrm{SVM}}\right), \\ P_{\mathrm{cond\_diode\_inv}} = V_{\mathrm{D(0)}} I_{\mathrm{om}} \left(\frac{1}{2\pi} - \frac{m_{\mathrm{v}} \cos(\varphi_{\mathrm{o}})}{8}\right) \\ \quad + r_{\mathrm{D}} I_{\mathrm{om}}^2 \left(\frac{1}{8} - \frac{m_{\mathrm{v}} \cos(\varphi_{\mathrm{o}})}{3\pi} - 2\pi F_{\mathrm{SVM}}\right), \end{cases} \quad (9)$$

$$F_{\mathrm{SVM}} = \frac{6\sqrt{3}}{\pi} \sum \left(\frac{\cos(k\varphi_0)}{k^5 - 5k^3 + 4k} - \frac{\cos(l\varphi_0)}{l^5 - 5l^3 + 4l}\right), \quad (10)$$

where, v_{ref} is the reference voltage, k denotes the harmonic order. Losses of the proposed converter are calculated by considering the following parameters,

$$\hat{U}_1 = \sqrt{2} \cdot 230\ \mathrm{V}, \hat{I}_2 = 15\ \mathrm{A}, f_s = 20\ \mathrm{kHz}, K_1 = \\ = 6.4 \frac{\mathrm{nJ}}{\mathrm{V}^2}, K_2 = 278.2 \frac{pJ}{AV^2}, K_3 = 229.5 \frac{\mu J}{V^2}. \quad (11)$$

The maximum loss is obtained at a firing angle $\frac{\pi}{3}$ and is calculated as

$$P_{tot,max} = \frac{3}{8\pi^2} f_s \cdot \left[6\sqrt{3}\pi \cdot \hat{I}_2 K_3 + \hat{U}_1^2 \cdot \left(3\sqrt{3} + 4\pi\right) * \left(\frac{9}{2}\sqrt{3}\hat{I}_2 K_2 + 2\pi K_1\right)\right] + \\ + \frac{1}{2}\hat{I}_2 \left[27K_2 \cdot \hat{U}_1^2 + 4\sqrt{3}\pi\left(K_3 + 3K_2 \cdot \hat{U}_1^2\right)\right] = 233\ \mathrm{W} \quad (12)$$

Here, f_s denotes the switching frequency, K_1, K_2, K_3 represent the constant parameters. The minimum loss is obtained at a firing angle $\frac{of\ 5\pi}{6}$ and is calculated as,

$$P_{tot,min} = \frac{3}{8\pi^2} f_s \cdot \left[8\pi \cdot \hat{I}_2 K_3 + \hat{U}_1^2 \cdot \left[\left(3\sqrt{3} + 4\pi\right) * \left(\frac{21}{2}\hat{I}_2 K_2 + 2\pi K_1\right) - \right.\right. \\ \left.\left. - \left(9 + 4\sqrt{3}\pi\right) \cdot \frac{3}{2}\sqrt{3}\hat{I}_2 K_2\right]\right] = 159\ \mathrm{W} \quad (13)$$

Similarly, the average value is 193 W, representing the DLO-based closed-loop control shown in Fig 2.

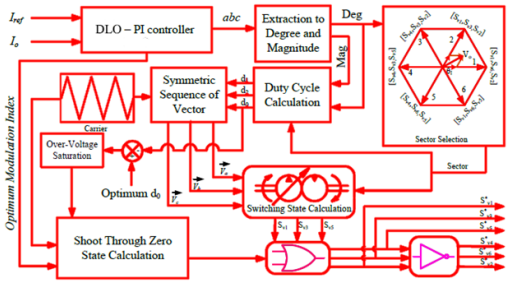

Fig. 2- Proposed DLO-based closed-loop control system

4. DLO CONTROL STRATEGY

In the realm of continuous optimization, the Dandelion optimizer has emerged among various swarm optimization algorithms. The seeds are sown to dozens of kilometers in the right conditions. Dandelion seeds travel under 4 stages *i.e.*, (i) Initial stage, (ii) Rising stage, (iii) Falling or Descending stage, and (iv) Final or Landing stage.

In the **Initial Stage**, it requires the initialization of population generation and iterative optimization. Each dandelion seed can be expressed in terms of population as

$$\text{popu} = \begin{cases} Y_1' \dots \dots \dots \dots \dots \dots Y_1^{Dim}, \\ , \\ , \\ , \\ Y_{pop}' \dots \dots \dots \dots \dots \dots Y_{pop}^{Dim}. \end{cases} \quad (13)$$

Dim is the variable dimension, while pop is the size of the dandelion seed population. Each seed solution is generated depending on the upper and lower bounds of a particular condition. Thus, the individual's ideal fitness value, Y_{elite}, is, $\mathrm{f}_{\mathrm{best}} = \min(\mathrm{f}(Y_{\mathrm{i}}))$

$$Y_{elite} = Y\left(\text{find}\left(\mathrm{f}_{\mathrm{best}} == f(Y_{\mathrm{i}})\right)\right). \quad (14)$$

Dandelion seeds must reach a certain height during the rising stage before attempting to fly away from their parent. Assume the condition to be a clear day with lognormal distribution with parameters (μ, σ^2). The mathematical expression is given by,

$$Y_{t+1} = Y_t + \beta * V_x * V_y * \ln X * (Y_s - Y_t), \quad (15)$$

where Y_t is the iterative position t of a dandelion seed, Y_s is the random position in selected search space,

$$\mathrm{Y}_s = \text{rand}(1, \text{Dim}) * (\text{Upper bound} - \text{Lower bound}) + \\ + \text{Lower bound} \quad (16)$$

$\ln X$ indicates the logarithmic normal distribution with mean 0 and variance 1, *i.e.*, $(\mu,\sigma^2) = (0,1)$. The mathematical formula for a lognormal distribution is,

$$\ln X = \begin{cases} \frac{1}{x\sqrt{2\pi}} \exp\left[-\frac{1}{2\sigma^2}(\ln x)^2\right], \\ x \geq 0 \\ 0, y < 0 \end{cases} \quad (17)$$

Equation (18) uses an adjustable parameter β to change each search step and is stated as:

$$\beta = \text{rand}() * \{(1/T)t^2 - (2/T)t + 1\}. \quad (18)$$

Here, t denotes the iteration count. β perturbates between [0,1] and it is nonlinear with a decrease reaching 0.

In the **Descending** stage, the DLO algorithm emphasizes the exploration stage. This ensures the population at a maximum community. Given by mathematical expression

$$\mathrm{Y}_{t+1} = Y_t - \beta * \alpha_t * (Y_{mean} - \beta * \alpha_t *), \quad (19)$$

where α_t denotes the Brownian motion, which is a random number, and Y_{mean} is the average position of the population

$$Y_{mean} = \frac{1}{pop} \sum_{i=1}^{pop} Y_i. \quad (20)$$

The erratic movement leads to a search that is likely to be near the global optimum.

In the **Final Stage**, depending on the initial and descending stage, the dandelion chooses the position to land. To converge accurately search agents borrow information in local neighborhoods with population evolution. Finally, a global position is reached,

$$\mathrm{Y}_{t+1} = Y_{\text{elite}} + \lambda * \beta * (Y_{elite} - \mathrm{Y}_t * \delta), \quad (21)$$

Y_{elite} is the i^{th} optimal dandelion seed position, λ function representing levy flight.

$$\lambda = \frac{(p * \omega * \sigma)}{|t|^{\frac{1}{\alpha}}}, \quad (22)$$

where α is a random number within [0,2], p is a constant approximated to 0.01, and ω and t are random numbers [0,1]

$$\sigma = \left[\frac{\Gamma(1+\alpha) * \sin(\frac{\pi\alpha}{2})}{\Gamma(\frac{1+\alpha}{2}) * \alpha * 2^{\frac{(\alpha-1)}{2}}}\right], \quad (23)$$

α is linearly increasing function δ

$$\delta = 2t/T. \quad (24)$$

To avoid excess optimization, a linearly increasing function is incorporated in (24).

5. SIMULATION RESULTS

The proposed method was implemented with MATLAB R2021a and verified across three conditions. The proposed system is tested under grid voltage distortions and grid voltage unbalance under the first two conditions, which are being conducted using the modular SVM controller.

Table 1

Performance comparison of the CMC and MUSMC

Wind velocity (m/s)	Generator output voltage (V)	frequency (Hz)	Conventional CMC		MUSMC	
			Output voltage (V)	Voltage transfer ratio	Output voltage (V)	Voltage transfer ratio
2	130	15.5	96	0.73	103	0.79
4	155	28.57	123	0.79	131	0.84
6	185	33.33	151	0.8	163	0.88
8	280	35.48	225	0.806	249	0.889
10	310	47.61	254	0.819	288	0.92
12	380	49.2	321	0.845	371	0.976

The third condition is the testing of the entire system with conventional and modular SVM methods. Table 1 shows the voltage transformation ratios for the suggested and traditional systems at various wind speeds. Table 2 depicts the comparative analysis of the voltage transfer ratio with proposed method and existing CMC, quasi-Z-USMC, Step up-USMC. When the wind velocity range increase the velocity transfer ration also increases. From the comparative analysis, the proposed method yields the highest voltage transfer ration than the existing methods.

Table 2

Comparative analysis of the voltage transfer ratio.

Wind velocity (m/s)		Conventional CMC	Quasi Z-USMC	Step up-USMC	Proposed MUSMC
2	0.73	0.76	0.785	0.79	
4	0.79	0.802	0.821	0.84	
6	0.8	0.823	0.861	0.88	
8	0.806	0.851	0.874	0.889	
10	0.819	0.897	0.907	0.92	
12	0.845	0.927	0.954	0.976	

To improve performance, the output current's THD must be reduced, and the reference current must be tracked constantly. This optimized control technique aims to reduce undesirable harmonic distortions in output current waveforms by optimizing the PI values and other regulating parameters. Table 3 shows that the proposed method creates less overshoot and takes much less rise and settling time than the different algorithms.

Table 3

Analysis of DLO with other methods.

Controller	Setpoint response			Load disturbance response		
	Mp %	tr	ts	Mp %	tr	ts
DLO − PI	10	0.08	0.16	9.3	0.09	0.18
PSO − PI	39	0.10	0.49	38	0.11	0.50
BA − PI	10	0.43	1.27	10	0.45	0.28
GA − PI	29	0.28	1.36	28	0.30	1.36

Figure 3 depicts how the system responds when controlled by various optimization-based PI controllers. The DLO approach responds faster with a shorter rising and settling time than the other optimization techniques. The DLO method is more advantageous than the other conventional methods because in DLO there are two sorts of dandelion populations (the core dandelion population and the assistance dandelion population), and they are both used to spread seeds, but in different ways. As a result, the DLO can prevent an untimely convergence.

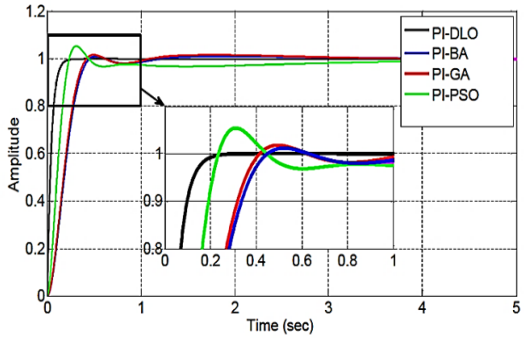

Fig. 3 – Response comparison of optimization-based PI controllers.

5.1. VALIDATION OF CONTROLLER PARAMETERS

The output vector's threshold value is set to open brackets $[0, 10^7]$ to get the most precise value.

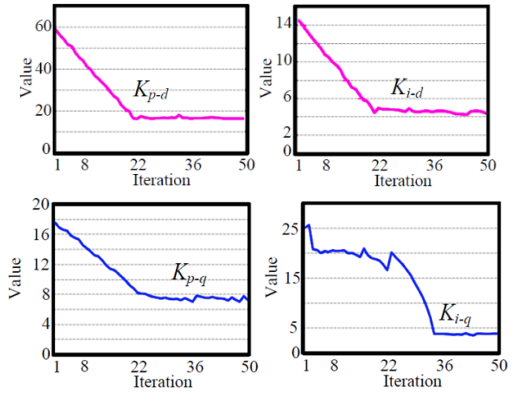

Fig.4- PI controller-tuned parameters using DLO.

Figure 4 depicts the findings obtained using the DLO method. There are a maximum of 600 rounds. Only the fifty important iterations are considered from the total number of iterations for better results. It is best to use 17.3218 and 3.8698 for the PI controller to control d and 7.6983 and 5.1796 for the PI controller to control q.

5.2. CASE 1: GRID VOLTAGE WITH HARMONIC DISTORTIONS

In the first case, the grid voltage is identified with 13% of the H_5 component and 10% of $the\ H_3$ component. H_5 and H_3 are the 5th and 3rd-order harmonics. Figure 5 shows the various outputs of the introduced system operating under case 1. with harmonic distortions, 5(a) the output waveform of grid voltage, 5(b) the sinusoidal stator current waveform, 5(c) presents the output waveform of the proposed MUSMC, 5(d) presents the reference dq current waveform and 5€ presents the actual dq current waveform. It is observed that the reference current does not contain harmonics. Therefore, the rotor currents presented in Fig. 5(f) appear to be sinusoidal, thus making a controlled current source operation. Figure 5(g) presents the ripple-free rotor output voltage waveform of phase "a".

5.3. CASE 2: UNBALANCED GRID VOLTAGE

In case 2, a voltage sag in phase "a" has been created at a period of 2ms. Due to the creation of voltage sag in phase "a" unbalanced stator voltages are observed in Fig. 6(a). Fig. 6(b) presents the stator current. Figure 6(c) presents the rotor current, and Fig. 6(d) presents the rotor phase voltage. It can be observed that the controller works effectively in producing the rotor currents without harmonics. Since the rotor currents are free from distortions, the stator currents also will be free from harmonic distortions and appear to be sinusoidal. Figure 7 presents the FFT analysis of rotor voltage and rotor current corresponding to phase "a". Due to the presence of a sag in phase "a" the 50 Hz element in the FFT analysis of Fig. 7(a). The 120 Hz components are used for compensating the sag. This 120 Hz , the component cancels the harmful sequence component produced due to sag. It creates a zero voltage, thereby preventing the circulation of unbalanced currents in the DFIG stator.

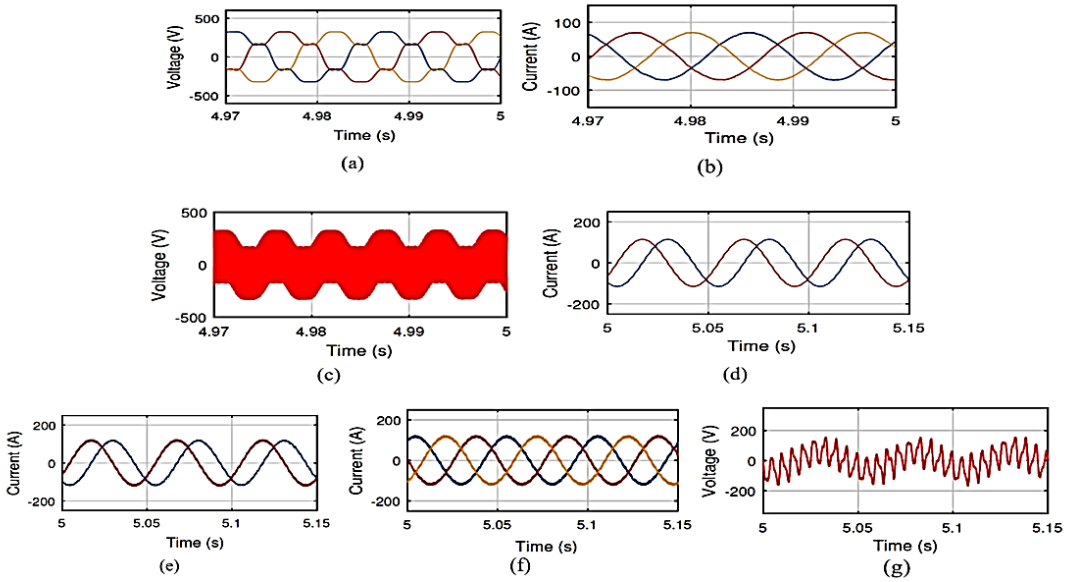

Fig. 5 – Simulation results of case 1 a) Stator voltage b) Stator current c) MUSMC output d) reference dq current e) actual dq current f) Rotor current g) Rotor a-phase voltage.

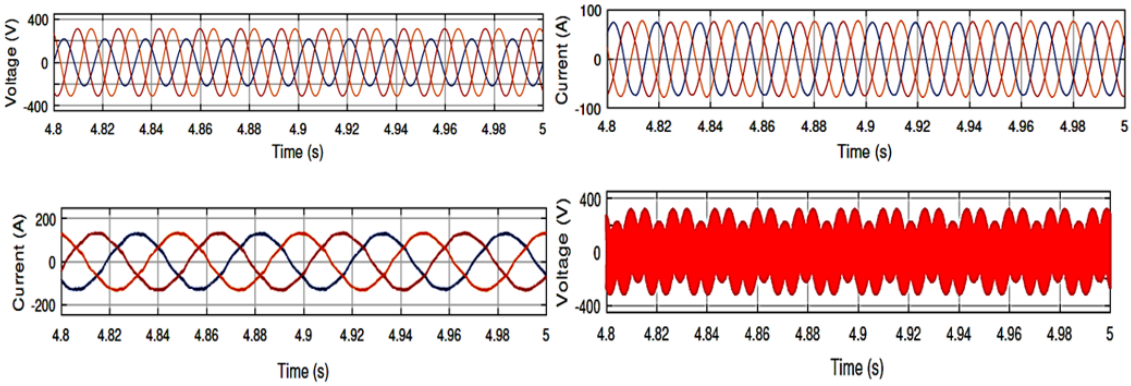

Fig. 6 – Simulation results of case 2 a) Stator voltage b) Stator current c) Rotor Current d) Rotor Phase Voltage.

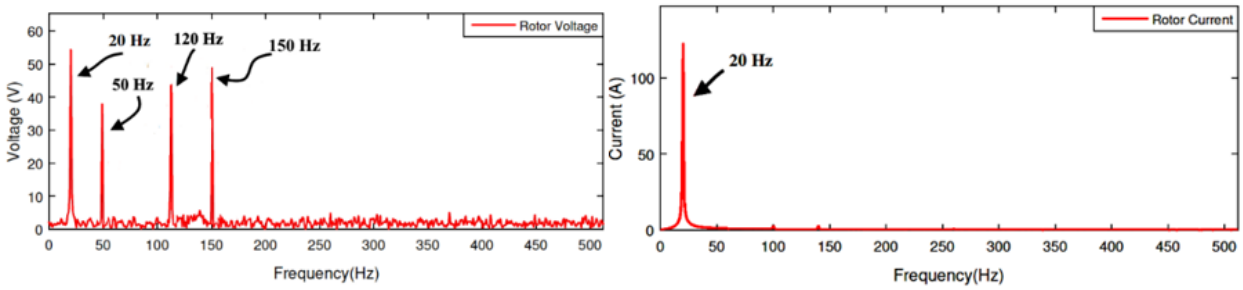

Fig. 7 – FFT analysis a) Rotor voltage b) Rotor current.

5. CONCLUSION

This paper presents the modified ultrasparse matrix converter (MUSMC) with the DLO algorithm to increase the quality of wind power and feed it into the system. The MUSMC is used to overcome this limitation and connect the DFIG-based WECS to the grid. The proposed system performance is simulated and tested in MATLAB/Simulink R2021a while considering harmonics in the grid, unbalanced grid, and modulation scheme changes. The ultra-sparse matrix converter (USMC) generally outperforms traditional direct and indirect matrix converters; however, the average USMC has a low voltage transformation ratio. The proposed technique adds a Z source network to the standard USMC to increase the voltage transformation ratio. In addition to that, while operating a modified USMC in rectifier mode, the switching state can be easily changed at zero current conditions. The simulation results show that the proposed modular control method with the MUSMC performs well under the three test cases, and the FFT analysis proves the superiority of the control strategy. According to the simulation result, the proposed method provides 0.9%, 1.2%, and 2.3% faster response than existing BA, GA, and PSO techniques. Future research could explore advanced modulation techniques to improve harmonic reduction, particularly under variable load conditions and grid disturbances.

ACKNOWLEDGMENTS

The author would like to express his heartfelt gratitude to the supervisor for his guidance and unwavering support during this research as well as his advice and support.

CREDIT AUTHORSHIP CONTRIBUTION

The authors confirm contribution to the paper as follows: study conception and design: Wencheslaus Vinil Dani, Michael Christudhas Jobin Christ; data collection: Wencheslaus Vinil Dani, Michael Christudhas Jobin Christ; analysis and interpretation of results: Wencheslaus Vinil Dani, Michael Christudhas Jobin Christ; draft manuscript preparation: Wencheslaus Vinil Dani, Michael Christudhas Jobin Christ. All authors reviewed the results and approved the final version of the manuscript.

Received on 18 October 2023

REFERENCES

1. D.S. Vanaja, A.A. Stonier, G. Mani, S. Murugesan, *Investigation and validation of solar photovoltaic-fed modular multilevel inverter for marine water-pumping applications.* Electrical Engineering, pp. 1–16 (2021).
2. R. Elumalai, *Maximum power quality tracking of artificial neural network controller-based double fed induction generator for wind energy conversion system,* Rev. Roum. Sci. Techn. – Électrotechn. Et Énerg., **69**, *2*, pp. 189–194 (2024).
3. G.R. Bruzinga, A.J. Sguarezi Filho, A. Pelizari, I. Oliani, *Comparison of analytical and numerical methods for PMSG design applied to D-type wind generators*, IEEE Latin America Transactions, 100 (XXX) (2022).
4. K. Gireeshma, S. Chandramohan, *A Review on LVRT and HVRT requirements and enhancement methods for DFIG wind turbines in INDIA*, International Virtual Conference on Power Engineering Computing and Control: Developments in Electric Vehicles and Energy Sector for Sustainable Future (PECCON), May, pp. 1–6 (2022).
5. R.A. Oliveira, M.H. Bollen, *Magnification of transients at the voltage dips starting and its impacts on DFIG-based wind power plants*, Electric Power Systems Research, **211**, 108244 (2022).
6. A. Ramalho, M.A. Vitorino, M. Correa, L.A.C. Costa, E. Braga-Filho, *New family of two-to-three-phase AC-AC indirect matrix converters with open-end rectifier stage*, IEEE Transactions on Industry Applications (2021).
7. B. Charaf, L. Hocine, M. Boubekeur, *A novel approach for controlling with a matrix converter*, Rev. Roum. Sci. Techn. – Électrotechn. Et Énerg., **68**, *1*, pp. 24–29 (2023).
8. O. Aydogmus, G. Boztas, R. Celikel, *Design, and analysis of a flywheel energy storage system fed by matrix converter as a dynamic voltage restorer*, Energy, **238**, 121687 (2022).
9. R. Wang, H. Hao, S. Yuan, X. Hui, *High-gain sparse three-level indirect matrix converter and its modulation strategy*, Journal of Power Electronics, **22**, *4*, 569–579 (2022).
10. S.A. Khanday, O.C. Sekhar, T.N. Mir, *Comparative study of three-phase AC/AC in-direct matrix converters: a review*, International Conference for Advancement in Technology (ICONAT), IEEE, 1–

6 (January 2022).
11. T. Malakar, V. Siva, S.K. Singh, *FPGA-Based Modulation Technique for Five-to-Three-Phase Ultra Sparse Matrix Converter,* Recent Trends in Electronics and Communication, Springer, Singapore, 1187–1199 (2022).
12. K. Nakamura Y. Zhang, T. Onchi, H. Idei, M. Hasegawa K. Tokunaga, K. Hanada, H. Chikaraishi, O. Mitarai, S. Kawasaki, A. Higashijima, *Quaternion Analysis of transient phenomena in matrix converter based on space-vector modulation*, Plasma and Fusion Research, **17**, 2405025–2405025 (2022).
13. V. Dahiya, G. Leena, *Analysis of predictive current control technique in wind energy conversion system,* Renewable Energy Optimization, Planning and Control, Springer*,* Singapore, pp. 101–111 (2022).
14. M. Selvi, P.M. J. Prathap, *Analysis & classification of secure data aggregation in wireless sensor networks*, International Journal of Engineering and Advanced Technology. **8**, *4*, pp. 1404–1407 (2019).
15. R. Belal, M. Flitti, M.L. Zegai, *Tuning of Pi speed controller in direct torque control of dual star induction motor based on genetic algorithms and neuro-fuzzy schemes*, Rev. Roum. Sci. Techn. – Électrotechn. Et Énerg., **69**, *1*, pp. 9–14 (2024).
16. K. Budo, T. Takeshita, *Experimental characteristics of capacitor voltage balancing control in modular matrix converter for isolated medium-voltage AC-DC converter*, 23rd European Conference on Power Electronics and Applications (EPE'21 ECCE Europe)*,* pp. 1–10 (2021).
17. H.F. Ahmed, M.S. El Moursi, B. Zahawi, K. Al Hosani, A.A. Khan, *Single-phase symmetric-bipolar-type high-frequency isolated buck-boost AC–AC Converter with continuous input and output currents*, IEEE Transactions on Power Electronics, **36**, *10*, pp.11579–11592 (2021).
18. N. Taheri H. Orojlo, F. Ebrahimi, *Damping controller design in offshore wind power plants to improve power system stability using fractional order PID controllers based on optimized exchange market algorithm*, Journal of Intelligent Procedures in Electrical Technology, **13**, *51*, pp. 91–110 (2022).
19. Y. Mousavi, G. Bevan, I.B. Kucukdemiral, A. Fekih, *Sliding mode control of wind energy conversion systems: Trends and applications*, Renewable and Sustainable Energy Reviews, **167**, 112734 (2022).
20. D. Shunmugham Vanaja, A.A. Stonier, *A novel PV-fed asymmetric multilevel inverter with reduced THD for a grid-connected system*, International Transactions on Electrical Energy Systems, **30**, *4*, e12267 (2020).
21. P.M.J. Prathap, V.G. Menon, *Survey on latest energy-based routing protocols for underwater wireless sensor networks*, Journal International Journal of Computer Networks and Wireless Communications (IJCNWC), **66** (2016).
22. D. Shunmugham Vanaja, A.A. Stonier *Grid integration of modular multilevel inverter with improved performance parameters*, International Transactions on Electrical Energy Systems, **31**, *1*, p.e. 12667 (2021).
23. M.A. Ebrahim, M. Becherif, A.Y. Abdelaziz, *Dynamic performance enhancement for wind energy conversion system using Moth-Flame Optimization based blade pitch controller*, Sustainable Energy Technologies and Assessments, **27**, 206–212 (2018).
24. Q. Wang, H. Xi, F. Deng, M. Cheng, G. Buja, *Design and analysis of genetic algorithm and BP neural network based PID control for boost converter applied in renewable power generations*, IET Renewable Power Generation, **16**, *7*, 1336–1344 (2022).
25. K. Aseem, S.S. Kumar, *Hybrid k-means grasshopper optimization algorithm based FOPID controller with feed-forward DC–DC converter for solar-wind generating system*, Journal of Ambient Intelligence and Humanized Computing, **13**, *5*, pp. 2439–2462 (2022).
26. S. Sharma, V.K. Tayal, *Optimised controller design for frequency control of a wind turbine driven doubly fed induction generator.* International Journal of Ambient Energy, pp. 1–10 (2022).
27. F. Amrane, A. Chaiba, B. Francois, B. Babes, *Real-time implementation of grid-connection control using robust PLL for WECS in variable speed DFIG-based on HCC*,. 5th International Conference on Electrical Engineering-Boumerdes (ICEE-B), 1–5 (2017). IEEE.
28. F. Amrane, A. Chaiba, B. Francois, B. Babes, *Real time implementation of grid-connection control using robust PLL for WECS in variable speed DFIG-based on HCC*, 5th International Conference on Electrical Engineering-Boumerdes (ICEE-B), pp. 1–5 (2017). IEEE.
29. B. Babes, O. Aissa, N. Hamouda, I. Colak, *Model based predictive direct torque and flux control for grid synchronization of a PMSG driven by a direct matrix converter,* 10th International Conference on Smart Grid (icSmartGrid), IEEE, pp. 208–213 (2022).
30. M. Israyelu, S. Sashidhar, *Hybrid switched inductor step-up ultra-sparse matrix converter for wind generator applications. In IECON*, Annual Conference of the IEEE Industrial Electronics Society, pp. 1–6, (2021). IEEE.
31. V. Siva, M. Raghuram, A. Singh, S.K. Singh, Y.P. Siwakoti, S*witching strategy to reduce inductor current ripple and common mode voltage in quasi Z-source ultra sparse matrix converter*, IEEE Journal of Emerging and Selected Topics in Industrial Electronics, **4**, *4*, pp. 1159–1169 (2023).
32. A. Appathurai, P. Deepa, *Design for reliability: A novel counter matrix code for FPGA based quality applications*, 6th Asia Symposium on Quality Electronic Design (ASQED), IEEE, pp. 56–61 (2015).
33. P.G. Sreelekshmi, S.C. Ramesh, Dingo Optimized Fuzzy CNN technique for efficient protein structure prediction, International Journal of Data Science and Artificial Intelligence, 01(02), 32–40 (2023).
34. A. Ahilan, P. Deepa, *Modified decimal matrix codes in FPGA configuration memory for multiple bit upsets*, International Conference on Computer Communication and Informatics (ICCCI), IEEE, pp. 1–5 (2015).
35. C. Senthil Singh, Sameena Naaz, G. Saranya, *IOT-centric data protection using deep learning technique for preserving security and privacy in cloud*, International Journal of Data Science and Artificial Intelligence, **2,** *3*, pp. 81–87 (2024).